Plasmonic transverse dipole moment in chiral fermion nanowires

Jinlyu Cao [1,2], H. A. Fertig,[1,2] and Luis Brey [3]
[1]*Department of Physics, Indiana University, Bloomington, Indiana 47405, USA*
[2]*Quantum Science and Engineering Center, Indiana University, Bloomington, Indiana 47408, USA*
[3]*Instituto de Ciencia de Materiales de Madrid, (CSIC), Cantoblanco, 28049 Madrid, Spain*

(Received 19 May 2022; revised 20 September 2022; accepted 29 September 2022; published 24 October 2022)

Plasmons are elementary quantum excitations of conducting materials with Fermi surfaces. In two dimensions they may carry a static dipole moment that is transverse to their momentum which is quantum geometric in nature, the quantum geometric dipole (QGD). We show that this property is also realized for such materials confined in nanowire geometries. Focusing on the gapless, intrasubband plasmon excitations, we compute the transverse dipole moment $\mathcal{D}_x$ of the modes for a variety of situations. We find that single chiral fermions generically host nonvanishing $\mathcal{D}_x$, even when there is no intrinsic gap in the two-dimensional spectrum, for which the corresponding two-dimensional QGD vanishes. In the limit of very wide wires, the transverse dipole moment of the highest velocity plasmon mode matches onto the two-dimensional QGD. Plasmons of multivalley systems that are time-reversal symmetric have a vanishing transverse dipole moment but can be made to carry nonvanishing values by breaking the valley symmetry, for example, via a magnetic field. The presence of a nonvanishing transverse dipole moment for nanowire plasmons in principle offers the possibility of continuously controlling their energies and velocities by the application of a static transverse electric field.

DOI: 10.1103/PhysRevB.106.165125

I. INTRODUCTION

Plasmons are fundamental excitations of metals, in which electronic charge oscillates against the fixed positively charged background of a material, with accompanying electric fields that allow for self-sustaining collective motion [1–4]. The behavior can be understood at a semiclassical level by solving Maxwell's equations in the presence of a frequency-dependent conductivity, which encodes information about the electron dynamics in the material [5]. Beyond their bulk realization, plasmons may be confined to the surfaces of some solids, with charge oscillations whose amplitudes evanesce quickly inside the material [6,7]. The development of two-dimensional electron systems in semiconductors [8] allowed such confined plasmons [9,10] to be realized with a degree of tunability not possible at the surface of a bulk material. In more recent years, the advent of van der Waals materials, particularly graphene, has greatly enriched the set of interesting physical possibilities for two-dimensional plasmons [11–16]. These include a myriad of applications and phenomena, in areas as diverse as terahertz radiation, biosensing, photodetection, quantum computing, and more [17–30].

Beyond all this, plasmons are interesting for basic physical reasons: they represent quantum, bosonic excitations of charged fermions with a Fermi surface [31,32]. Their quantum nature can in principle become evident through manifestations of their quantum geometry. In two-dimensional materials this nature becomes particularly important because it makes possible strong light-matter interactions, allowing for probes well below the wavelength of light at plasmonic frequencies [33–36]. Moreover, Berry curvature in the electronic structure of the host material may lead to chiral behavior even in the absence of a magnetic field [37]. More generally quantum effects may lead to nonreciprocal behavior of plasmons [38,39]. Indeed, in some systems plasmons have internal structure in the form of a static dipole moment, which leads to nonreciprocity in their scattering from point impurities or other circularly symmetric scattering centers [40]. This quantum geometric dipole (QGD) moment is present in collective excitations of insulators—excitons—as well [41]. In both cases the QGD is transverse to the momentum of the collective mode.

An interesting question is whether effects of this transverse dipole moment can be directly observed, independent of its impact on scattering. One way to approach this question is to consider its effect on plasmons in a confined geometry, which may tend to orient the dipole moment in a way that allows coupling to electric fields. The simplest such geometry is quasi-one-dimensional, in which one might expect the dipole moment to align perpendicular to the channel axis. This is the subject of our study. Our principle results demonstrate that such transverse dipole moments are relatively common in this geometry: they can appear even when the corresponding two-dimensional bulk system does not carry a QGD.

In what follows, we consider a system that supports a plasmonic QGD, a layer of gapped chiral fermions, in which the single-particle states are confined to be within a narrow channel. Such systems arise naturally in the context of transition-metal dichalcogenides (TMDs) [42] and for graphene, which, when placed on a boron nitride or silicon carbide substrate, may develop a gap at its Dirac points as large as 0.5 eV [43,44]. The single-particle electronic structure of such nanowires is sensitive to the precise nature of

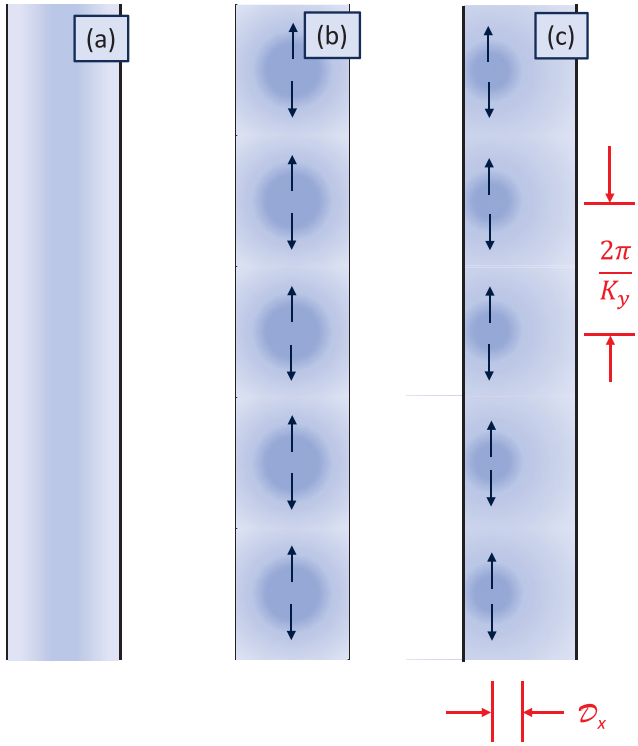

FIG. 1. Sketch of a plasmon mode in a nanowire. (a) Ground-state density, with heavier shading indicating regions of higher electron density. (b) Snapshot of a plasmon mode in a nanowire of a conventional electron gas. Regions of heavier shading indicate larger electron density. Arrows in interior of wire indicate direction of current at that moment in time. The charge density oscillates spatially with wave vector $2\pi/K_y$, where K_y is the longitudinal momentum. (c) Snapshot of a plasmon mode in a nanowire of chiral fermions. The oscillating charge density is shifted transverse to the wire axis, yielding a dipole moment $\mathcal{D}_x$.

their edges [45–48] and may or may not involve the mixing of valleys [46,49]. For simplicity, our studies focus on infinite mass boundary conditions [50] for which there is no such valley mixing.

Plasmons in nanowires of chiral fermions [51] share many properties with those of scalar fermions [52,53]. Prominent among these are the presence of collective modes with an essentially linear dispersion and gapped intersubband modes. As we explain below, for a single chiral fermion, all these modes support transverse dipole moments with magnitude proportional to the longitudinal momentum of the plasmon. This orthogonality of the dipole moment and momentum is exactly as one finds for the QGD in two dimensions [40,41]. A sketch of this phenomenon is illustrated in Fig. 1. Interestingly, in these quasi-one-dimensional systems it appears even when there is no intrinsic gap in the spectrum, so that the QGD vanishes in the corresponding two-dimensional system [40,41], the gaps introduced by the transverse confinement stabilize the dipole moment.

Another feature of quasi-one-dimensional chiral fermions is that they may host edges states. Because the charge associated with these states is located near the channel edges, they potentially could have important consequences for the transverse dipole moment hosted by a plasmon state. We find generically that their effect is more quantitative than qualitative, but under some circumstances they can distinguish the number of plasmon modes with significant nonvanishing dipole moment values.

For systems with pairs of Dirac points connected by time-reversal symmetry, the transverse dipole moment vanishes, but nonvanishing values can be introduced into their plasmons by breaking this symmetry, for example, with a magnetic field. An interesting physical consequence of this physics is that this dipole moment can be coupled to a transverse electric field [54], allowing a degree of continuous control over the plasmon frequency and velocity that is unavailable in other nanowire systems.

This article is organized as follows. In Sec. II we discuss the single-particle wave functions for the confined states, and, when appropriate, for edge states of the massive chiral fermions we consider, assuming infinite mass boundary conditions. These states are the system-specific inputs to the calculations of plasmon modes. In Sec. III we explain our method for deriving the plasmon modes, both their energies and wave functions. The latter are used to compute dipole moments for the states, and we explain how this is done at the end of this section. A description of our numerical results follows in Sec. IV. We begin there by presenting results for a generic system, and then for parameters relevant to TMD materials, showing that the latter are somewhat unusual in having many modes with different dispersions but the same dipole moment. We then demonstrate that, for large system widths, the dipole moments tend to the values expected of two-dimensional systems. Finally, we consider more realistic TMD systems with two valleys, for which the transverse dipole moment must vanish when there is time-reversal symmetry. We show that introducing a magnetic field breaks the symmetry between valleys and allows a dipole moment to emerge. Finally, we conclude in Sec. V with a summary of our results, discussions of their experimental relevance, as well as interesting open questions.

Our paper also contains three Appendixes. Appendix A presents further details of how the single-particle states are derived. In Appendix B we explain qualitatively why there are multiple gapless plasmon modes in the systems we consider, focusing on the case of a system with two occupied transverse states as an example. Finally, Appendix C presents an explicit expression for the plasmon transverse dipole moment, which is appropriate for infinite mass boundary conditions, showing how under appropriate circumstances modes of different energies can have the same dipole moment.

II. CHIRAL FERMIONS ON A NANOWIRE: SINGLE-PARTICLE STATES

We begin by deriving the single-particle states for our nanowire models. The Hamiltonian we adopt for the noninteracting system in two dimensions is

$$H_0^\tau = \begin{pmatrix} m & -i\tau\partial_x - \partial_y \\ -i\tau\partial_x + \partial_y & -m \end{pmatrix}, \tag{1}$$

where $\tau = \pm 1$ indicates a valley degree of freedom, where in TMD materials $\tau = 1(-1)$ corresponds to the $K(K')$ valley.

We have adopted units such that $\hbar = v_F = 1$, where v_F is the velocity of the chiral particles in the absence of the mass parameter m. Its spectrum has a gap $\Delta = 2m$. This Hamiltonian is an appropriate long-wavelength description of TMD materials when excitations involving spin flips are ignored, and in the limit $m \to 0$ it also describes the single-particle physics of graphene [42,55,56]. Eigenstates of H_0 consist of right- and left-moving solutions in the $\hat{x}$ direction,

$$\begin{pmatrix} E+m \\ \pm\tau k_x + ik_y \end{pmatrix} e^{\pm ik_x x + ik_y y},$$

with energies

$$E = \sqrt{m^2 + k_x^2 + k_y^2}. \tag{2}$$

We choose an orientation in which the electrons are confined in the $\hat{x}$ direction and are free to move along $\hat{y}$. To confine the electrons, we adopt for simplicity infinite mass boundary conditions [50],

$$\left.\frac{\psi_1}{\psi_2}\right|_{x=0,L} = \pm i\lambda_0, \tag{3}$$

where $\lambda_0 = \mathrm{sgn}(C)$ is the sign of the Chern number outside the wire, and in writing this we have assumed $m \geqslant 0$. (Details of how one arrives at Eq. (3) are presented in Appendix A.) Note that, without loss of generality, we may assume a Chern number (of magnitude 1/2 [57]) for each valley in the material (i.e., inside the wire) with the sign of λ given by τ. This choice of boundary condition has the advantage of admitting confined solutions without admixing valleys, but the resulting confined states depend on their momentum k_y along the wire. This latter property is generic for chiral fermions [46,48,51], although in the special case where there are only two valleys, with equal momentum components along the wire direction, this momentum dependence is lifted [46] (at the cost of admixing valleys). The momentum dependence of the confined wave functions is a significant difference from the typical situation for electrons with scalar single-particle states [52]. Note that the parameter λ_0 enters the boundary condition, because one must choose the mass term outside the wire to tend to either ∞ or $-\infty$, and the choice of this sign determines whether the wire supports edge states, as we discuss further below.

Eigenstates of H_0 which satisfy the boundary conditions have the form (see Appendix A)

$$\begin{aligned}\vec{\psi}^{\tau}_{\vec{k}}(\vec{r}) = &A(\tau;\vec{k})\begin{pmatrix} E+m \\ \tau k_x + ik_y \end{pmatrix} e^{ik_x x + ik_y y} \\ &+ B(\tau;\vec{k})\begin{pmatrix} E+m \\ -\tau k_x + ik_y \end{pmatrix} e^{-ik_x x + ik_y y},\end{aligned} \tag{4}$$

with

$$A(\tau;\vec{k}) = \tau N\sqrt{(E+m)^2 + (\tau k_x - ik_y)^2}\sqrt{m + i\lambda_0\tau k_x}, \tag{5}$$

$$B(\tau;\vec{k}) = -\tau N\sqrt{(E+m)^2 + (\tau k_x + ik_y)^2}\sqrt{m - i\lambda_0\tau k_x}, \tag{6}$$

with a normalization constant given by

$$N = \left\{8L_y E(E+m)^2\left[L\left(m^2 + k_x^2\right) + \lambda_0\tau m\right]\right\}^{-1/2}, \tag{7}$$

in which L_y and L are the length and the width of the wire, respectively. The allowed values of k_x satisfy the transcendental equation

$$e^{2ik_x L} = \frac{m - i\lambda_0\tau k_x}{m + i\lambda_0\tau k_x}, \tag{8}$$

which in turn quantizes their values,

$$k_x L = -\lambda_0\tau \arctan\left(\frac{k_x}{m}\right) + n\pi, \tag{9}$$

where $n = 1, 2, 3, \ldots$.

In addition to these confined states, there may also be edge states, depending on the relative sign of the wire and the vacuum Chern numbers. Potentially these could be important, as their location near the sample edges suggests they can make large dipole moment contributions. Thus in our calculations below we will consider both systems with and without edge states. We will see that ultimately in most cases their impact is quantitative but not qualitative.

In systems with time-reversal symmetry, edge states come in pairs on each edge running in opposite directions, with the member of each pair associated with one or the other valley. For systems with a single chiral fermion, for which time-reversal symmetry is necessarily broken, a single edge state is present on each edge. These edge states exist only when the wire material and vacuum are topologically distinct, i.e., the signs of their Chern numbers are opposite,

$$\lambda_0\lambda = -1. \tag{10}$$

The edge states correspond to evanescent solutions of the Hamiltonian equation (see Appendix A) with wave functions

$$\begin{aligned}\vec{\psi}^{\tau}_{0,\vec{k}}(\vec{r}) = &A_0(\tau;\vec{k})\begin{pmatrix} m+E \\ i(\tau k_x + k_y) \end{pmatrix} e^{-k_x x + ik_y y} \\ &+ B_0(\tau;\vec{k})\begin{pmatrix} m+E \\ i(-\tau k_x + k_y) \end{pmatrix} e^{k_x x + ik_y y},\end{aligned} \tag{11}$$

and

$$A_0(\tau) = \tau\sqrt{\frac{[(m+E)^2 - (\tau k_x - k_y)^2](m+k_x)}{8E(E+m)^2 L_y\left[m - L\left(m^2 - k_x^2\right)\right]}}, \tag{12}$$

$$B_0(\tau) = -\tau\sqrt{\frac{[(m+E)^2 - (\tau k_x + k_y)^2](m-k_x)}{8E(E+m)^2 L_y\left[m - L\left(m^2 - k_x^2\right)\right]}}, \tag{13}$$

and energy

$$E = \sqrt{m^2 - k_x^2 + k_y^2}. \tag{14}$$

In these expressions the evanescent wave vector k_x satisfies the transcendental equation

$$e^{-2k_x L} = \frac{|m| - k_x}{|m| + k_x}. \tag{15}$$

Note that Eq. (15) only has solutions when the wire is wider than a minimal value (L^*), given by

$$L^* = \frac{\hbar v_F}{m}, \tag{16}$$

where we have replaced the explicit functional dependence on $\hbar v_F$. Examples of the single-particle dispersions relevant to

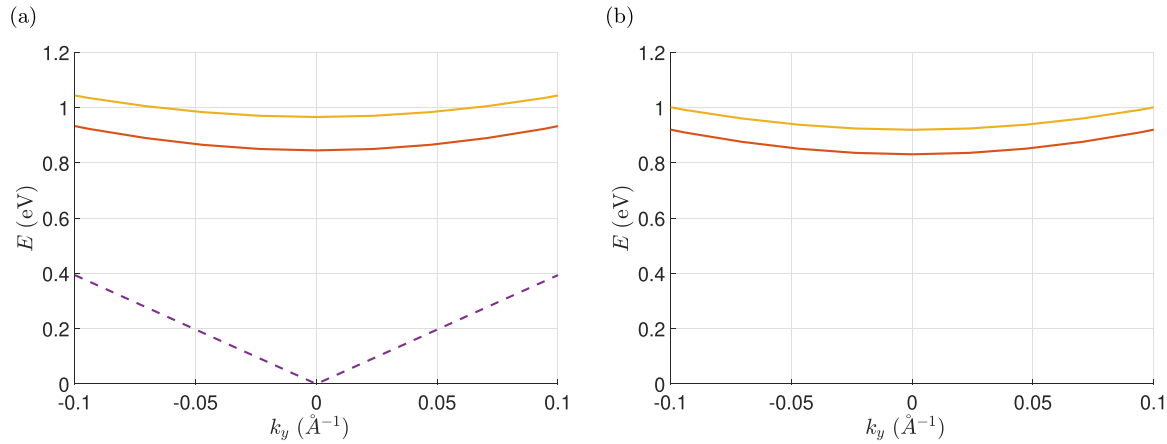

FIG. 2. (a) Lowest three positive-energy electric subbands for a single-valley chiral fermion with two confined states (solid lines) and an edge state (dashed line). The vacuum and wire have opposite Chern number signs $\lambda\lambda_0 = -1$. The half gap $m = 0.8$eV, wire width is $L = 50$Å, $v_F\hbar = 3.39\text{eV}\cdot$Å. (b) Lowest two positive-energy electric subbands for a single-valley chiral fermion with no edge state. The vacuum and wire have the same Chern number signs, $\lambda\lambda_0 = 1$. The half gap $m = 0.8$ eV, wire width is $L = 50$Å, $v_F\hbar = 3.39$ eV $\cdot$ Å.

our model are given in Figs. 2(a) and 2(b). Knowing how to construct these wave functions and energies, we next describe how they are used to compute the plasmon modes and their dipole moments.

III. PLASMON WAVE FUNCTIONS, ENERGIES, AND DIPOLE MOMENTS

In our study we are interested in the intrinsic dipole moment of plasmon states of a one-dimensional channel. Most previous studies of these focus on the dielectric function, as computed in the random phase approximation (RPA) [52,58,59]. This reveals the plasmon frequencies and their impact on the charge response of the system to applied electric fields. For our purpose we need access to the plasmon wave functions. The approach we adopt casts the plasmon wave function as a linear combination of particle-hole excitations around a Fermi sea ground state. While equivalent to RPA, it is best understood as a time-dependent Hartree approximation. In this section we explain how this approach is implemented and how the intrinsic transverse dipole moment may be extracted from it.

A. Hamiltonian and plasmon raising operator

Our Hamiltonian is a sum of single-particle and interaction parts, $\hat{H}_0 + \hat{V}$. The first of these is

$$\hat{H}_0 = \sum_m \sum_{k_y} \sum_{\tau,s} E_{m,\tau}(k_y) c^\dagger_{m,\tau,s}(k_y) c_{m,\tau,s}(k_y), \tag{17}$$

where $c^\dagger_{m,\tau,s}(k_y)$ creates an electron in subband m with longitudinal momentum k_y, with valley and spin indices τ and s, respectively. $E_{m,\tau}(k_y)$ is the single-particle energy, as computed in the previous section. For the interaction term we write

$$\hat{V} = \frac{1}{2}\sum_{s,s'} \int d^2r \int d^2r' : \vec{\Psi}^\dagger_s(\vec{r}) \cdot \vec{\Psi}_s(\vec{r}) V(\vec{r}-\vec{r}') \times \vec{\Psi}^\dagger_{s'}(\vec{r}') \cdot \vec{\Psi}_{s'}(\vec{r}') : \tag{18}$$

where the (vector) field operator $\vec{\Psi}^\dagger_s(\vec{r})$ creates an electron of spin s in the two orbitals of the chiral fermion system at the location $\vec{r}$, and $: \hat{\mathcal{O}} :$ denotes normal ordering of an operator $\hat{\mathcal{O}}$. We expand the field operator in terms of single-particle wire states,

$$\vec{\Psi}_s(\vec{r}) = \sum_{n,k_y,\tau} c_{n,\tau,s}(k_y) \vec{\psi}^\tau_{\vec{k},s}(\vec{r}). \tag{19}$$

In writing this we have identified $\vec{k} \equiv (k_x(n), k_y)$, allowing us to adopt a simplified indexing for the single-particle states $\vec{\psi}^\tau_{\vec{k},s}(\vec{r})$ which correspond to the states annihilated by $c_{n,\tau,s}(k_y)$. Adopting the same notation for these annihilation operators, $c_{\vec{k},\tau,s} \equiv c_{n,\tau,s}(k_y)$, brings the interaction to a form which may be written as

$$\hat{V} = \sum_{s,s'} \sum_{\substack{n_1,n_2,n_3,n_4 \\ k_{y1},k_{y2},k_{y3},k_{y4} \\ \tau_1,\tau_2,\tau_3,\tau_4}} V^{\tau_1,\tau_2,\tau_3,\tau_4}_{\vec{k}_1,\vec{k}_2,\vec{k}_3,\vec{k}_4} c^\dagger_{\vec{k}_1,\tau_1,s'} c^\dagger_{\vec{k}_2,\tau_2,s} c_{\vec{k}_3,\tau_3,s} c_{\vec{k}_4,\tau_4,s'}, \tag{20}$$

where $V^{\tau_1,\tau_2,\tau_3,\tau_4}_{\vec{k}_1,\vec{k}_2,\vec{k}_3,\vec{k}_4} = \frac{1}{2}\int d^2r \int d^2r' \vec{\psi}^{\tau_1}_{\vec{k}_1}(\vec{r})^* \cdot \vec{\psi}^{\tau_4}_{\vec{k}_4}(\vec{r}) V(\vec{r}-\vec{r}') \vec{\psi}^{\tau_2}_{\vec{k}_2}(\vec{r}')^* \cdot \vec{\psi}^{\tau_3}_{\vec{k}_3}(\vec{r}')$. In writing this we have taken note of the fact that for each subband there is a single quantized transverse momentum magnitude, $k_x(n)$, whose states with positive and negative values are admixed to form the transverse states discussed in the last section.

In what follows we adopt a contact interaction $V(\vec{r}-\vec{r}') = u_0\delta(\vec{r}-\vec{r}')$. This yields intrasubband plasmon modes that disperse linearly with longitudinal plasmon momentum K_y. If a $1/r$ potential is instead used, one expects to find $\omega(K_y) \sim K_y \ln K_y$ for at least one gapless plasmon mode; however, in practice the divergence of the slope is extremely difficult to see [52]. Thus the contact interaction introduces significant simplification in the computation of the matrix elements, without loss of any essential qualitative behavior in the plasmon mode. In practice, we choose the value of u_0 to match results for the slope of a plasmon mode as computed using the Coulomb interactions in a graphene system [60].

Collective excitations of the system can be obtained from operators satisfying the equation [31,61]

$$\left[\hat{H}, \hat{Q}^{\dagger}_{K_y}\right] = \hbar\omega_{K_y}\hat{Q}^{\dagger}_{K_y}. \tag{21}$$

In general, analytic solutions to Eq. (21) are not available. However, in the case of plasmons, corresponding to charge density excitations in the system, one may approximate the form of the plasmon raising operator $\hat{Q}^{\dagger}_{K_y}$ as a linear combination of single particle-hole pairs [31],

$$\hat{Q}^{\dagger}_{K_y} \equiv \sum_{m_1,m_2,k'_y,\tau,s} a_{m_1,m_2,\tau}(k'_y;K_y)c^{\dagger}_{m_1,\tau,s}(K_y+k'_y)c_{m_2,\tau,s}(k'_y), \tag{22}$$

and then treat the commutator $[\hat{V}, \hat{Q}^{\dagger}_{K_y}]$ in the time-dependent Hartree approximation:

$$\begin{aligned}\left[\hat{V}, \hat{Q}^{\dagger}_{K_y}\right] \approx 2\sum_{s,s'}\sum_{n_1,n_2,n_3,n_4}\sum_{\tau_1,\tau_4,\tau}\sum_{k_{y1},k'_y} & \\ \times\, V^{\tau_1,\tau,\tau,\tau_4}_{n_1,n_2,n_3,n_4}(K_y+k'_y,k_{y1},K_y+k_{y1},k'_y) & \\ \times\, a_{n_3,n_2,\tau,s}(k_{y1};K_y)c^{\dagger}_{n_1,\tau_1,s'}(K_y+k'_y) & \\ \times\, c_{n_4,\tau_4,s'}(k'_y)[n_F(n_2,k_{y1},\tau) & \\ - n_F(n_3,K_y+k_{y1},\tau)]. &\end{aligned} \tag{23}$$

Together with the commutator involving the single-particle Hamiltonian $\hat{H}_0$, one arrives at an eigenvalue equation for the particle-hole weights $a_{n_1,n_2,\tau,s}(k_y;K_y)$ and the plasmon frequency $\omega(K_y)$:

$$\begin{aligned}2\sum_{n_1,n_2}\sum_{k_{y1}}\sum_{\tau,s} & V^{\tau',\,\tau,\,\tau,\,\tau'}_{n'_1,n_2,n_1,n'_2}(K_y+k'_y,k_{y1},K_y+k_{y1},k'_y) \\ & \times a_{n_1,n_2,\tau,s}(k_{y1};K_y)[n_F(n_2,k_{y1},\tau)-n_F(n_1,K_y+k_{y1},\tau)] \\ & = \left[\omega_{K_y} - E_{n'_1,\tau'}(K_y+k'_y) + E_{n'_2,\tau'}(k'_y)\right]a_{n'_1,n'_2,\tau',s'}(k'_y;K_y).\end{aligned} \tag{24}$$

In this work we work strictly in the zero-temperature limit, so that $n_F(n,k_y,\tau) = 1(0)$ if the state (n,k_y,τ) is occupied (unoccupied) in the ground state.

We solve Eq. (24) numerically by retaining a discrete set of points in the k_y sum so that it becomes a matrix eigenvalue equation. Because we are interested in the lowest-lying plasmon modes, we further simplify the equation by retaining only intraband particle-hole excitations, so that we take $a_{n_1,n_2,\tau,s}(k_y;K_y) \neq 0$ only when $n_1 = n_2$; we have verified that keeping intersubband excitations has little effect on our results. We have further verified that increasing the number of k_y points used for the results reported below have little effect on them.

B. Plasmon dipole moment

In previous work [40,41] we demonstrated that two-body excitations, including excitons and plasmons, may carry an internal dipole moment that is tied to the quantum geometry of their wave functions. One sees this by defining Berry connections specific for the electrons ($\alpha = 1$) and holes ($\alpha = 2$),

$$\boldsymbol{\mathcal{A}}^{(\alpha)}(\mathbf{K}) = i\langle u_{\mathbf{K},\alpha}|\vec{\nabla}_{\mathbf{K}}|u_{\mathbf{K},\alpha}\rangle$$

with

$$|u_{\mathbf{K},\alpha}\rangle = e^{i\mathbf{K}\mathbf{r}_{\alpha}}|\Phi_{\mathbf{K}}\rangle\,,$$

where $|\Phi_{\mathbf{K}}\rangle$ is the wave function of the excited state. These connections can be directly related to the average electric dipole moment $\mathbf{d}$ of a plasmon,

$$\begin{aligned}\mathbf{d} &= e\langle\Phi_{\mathbf{K}}|\mathbf{r}_1 - \mathbf{r}_2|\Phi_{\mathbf{K}}\rangle \\ &= ie[\langle u_{\mathbf{K},\mathbf{1}}|\vec{\nabla}_K|u_{\mathbf{K},\mathbf{1}}\rangle - \langle u_{\mathbf{K},\mathbf{2}}|\vec{\nabla}_K|u_{\mathbf{K},\mathbf{2}}\rangle] \\ &= e[\boldsymbol{\mathcal{A}}^{(1)}(\mathbf{K}) - \boldsymbol{\mathcal{A}}^{(2)}(\mathbf{K})] \equiv e\boldsymbol{\mathcal{D}}(\mathbf{K}),\end{aligned} \tag{25}$$

where $\boldsymbol{\mathcal{D}}$ is the quantum geometric dipole. This quantity is relevant to plasmons because they may be understood as particle-hole excitations around a Fermi surface. In a two-dimensional system one finds $\boldsymbol{\mathcal{D}}(\mathbf{K})$ is orthogonal to $\mathbf{K}$, and for small K it is linear in K. This geometry suggests that when plasmons carry a nonvanishing $\boldsymbol{\mathcal{D}}$ in a two-dimensional material, plasmons confined to a one-dimensional channel of the same system may carry a transverse dipole moment. We can check this by computing the plasmon dipole moment directly. For a wire oriented along the $\hat{y}$ direction, following the reasoning above, for a plasmon state $|\Phi_{K_y}\rangle$ with momentum K_y along the wire one may write

$$\mathcal{D}_x(K_y) = \mathcal{A}^{(1)}_x - \mathcal{A}^{(2)}_x = \left\langle\Phi_{K_y}\middle|x_e - x_h\middle|\Phi_{K_y}\right\rangle. \tag{26}$$

Recalling the notation above in which a vector $\vec{k} = (k_x(n), k_y)$ specifies an electron state with longitudinal momentum k_y in a transverse state n, we write $\vec{\psi}^{\tau}_{\vec{k}} \to \vec{\psi}^{\tau}_{n,k_y}$, yielding an explicit expression,

$$\begin{aligned}\mathcal{D}_x(K_y) = \sum_{\substack{m_1,m_2,\\ m'_1,m'_2}}\sum_{k_y,\tau,s} & a^{*}_{m'_1,m'_2,\tau,s}(k_y;K_y)a_{m_1,m_2,\tau,s}(k_y;K_y) \\ & \times\left(\delta_{m_2,m'_2}\int x\vec{\psi}^{\tau *}_{m'_1,k_y+K_y}(\vec{r})\cdot\vec{\psi}^{\tau}_{m_1,k_y+K_y}(\vec{r})d^2r\right. \\ & \left. - \delta_{m_1,m'_1}\int x\vec{\psi}^{\tau}_{m'_2,k_y}(\vec{r})\cdot\vec{\psi}^{\tau *}_{m_2,k_y}(\vec{r})d^2r\right).\end{aligned} \tag{27}$$

In our numerical calculations, Eq. (27) is used to compute the dipole moment of a plasmon state. As we shall see, one finds that plasmons of a single chiral Dirac fermion nanowire *generically* have nonvanishing $\mathcal{D}_x(K_y)$, but with increasing wire width, this vanishes unless the corresponding two-dimensional system has a nonvanishing quantum geometric dipole. Having explained in this and the previous section how the plasmons and their dipole moments can be computed, we now turn to our numerical results.

IV. RESULTS

In this paper we focus on intraband plasmons, which for our contact interaction disperse linearly with momentum from zero energy. In general, we find that the number of such gapless plasmon modes is equal to the number of subbands which cross the Fermi energy, all of which may carry nonvanishing transverse dipole moments. We begin by considering the computationally simplest case of a single chiral fermion

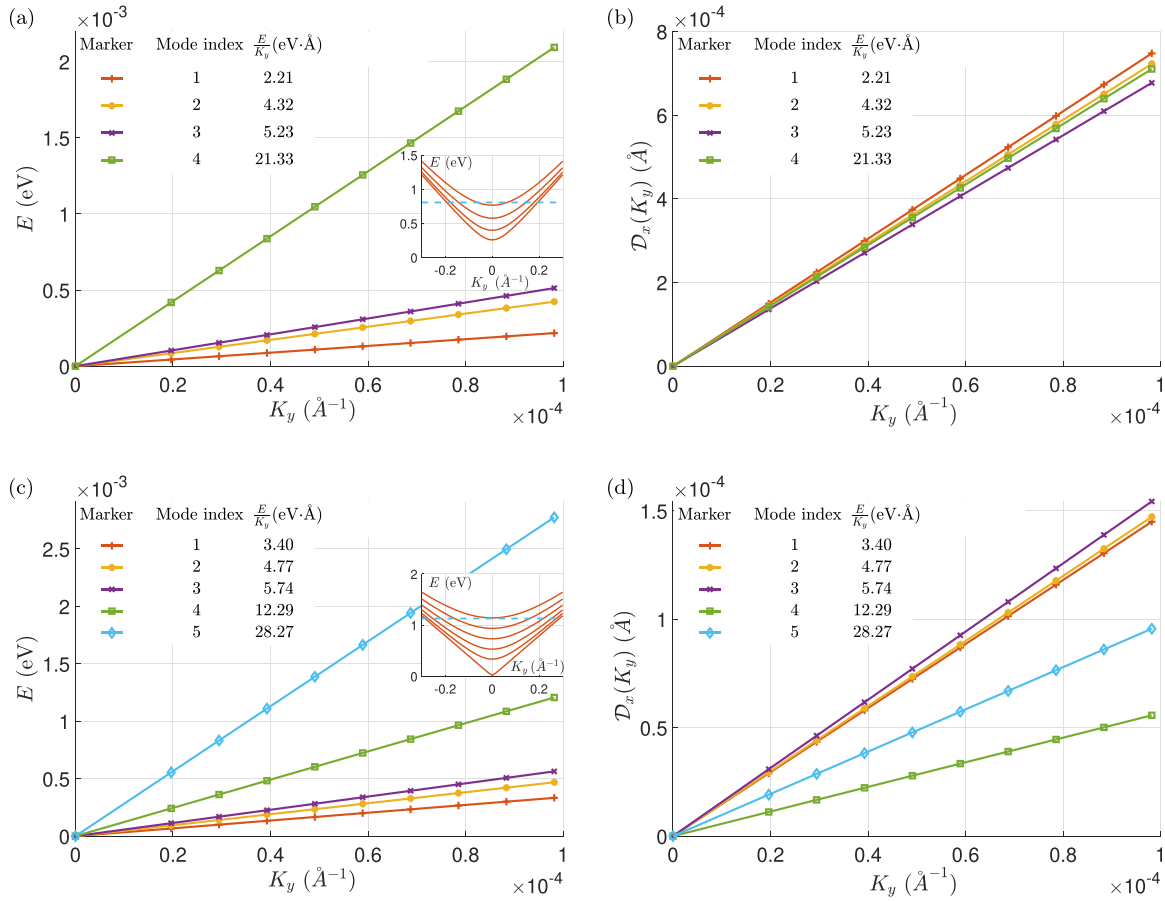

FIG. 3. Intraband plasmon energies and transverse dipole moments for K valley excitations. The wire width is $L = 60$Å, assumed gap $\Delta = 0.4\,\text{eV}$, $v_F\hbar = 3.94\,\text{eVÅ}$, Fermi energy $\varepsilon_F = 0.806\,\text{eV}$ for (a) and (b), Fermi energy $\varepsilon_F = 1.128\,\text{eV}$ for (c) and (d). (a) Plasmon energies when four subbands are occupied (no edge state due to boundary condition). There are four plasmon modes in total. (b) Transverse dipole moments corresponding to (a). (c) Plasmon energies when $5(= 4 + 1)$ subbands (including an edge state) are occupied. (d) Transverse dipole moments corresponding to (b). Insets: The single-particle spectrum and the dashed line indicating the Fermi energy.

flavor. In principle, such a system might be created on the surface of a topological insulator infused with ferromagnetically ordered dopants that gap the surface states everywhere except in a narrow channel, where plasmons can be hosted. We also consider single chiral fermions for parameters similar to those of TMD materials, for which we find that nearly all the modes have the same dipole moment. An exception to this behavior occurs when there are edge states, in which case there is a single plasmon mode with nearly vanishing dipole moment.

A surprising aspect of our results is that transverse dipole moments seem to occur rather ubiquitously for the quasi-one-dimensional chiral fermions we examine, whereas in two dimensions one finds a nonvanishing QGD only when the single-particle Hamiltonian carries a nonvanishing Chern number [40]. To understand this we consider the limit of wide ribbon widths and find that indeed the transverse dipole moment quantitatively matches the two-dimensional QGD, so that there is no contradiction in these results.

Finally, for this section we turn to more common situations for nanoribbons of van der Waals materials, for which the effects of multiple valleys and time-reversal symmetry lead to a vanishing transverse dipole moment. We show that this can be made nonvanishing by breaking the symmetry between valleys with a magnetic field.

A. Single chiral fermion

Our model Hamiltonian for a single chiral fermion is $\hat{H} = \hat{H}_0 + \hat{V}$, with $\hat{H}_0$ and $\hat{V}$ given by Eqs. (17) and (18), respectively, in which only a single-valley flavor τ is retained. For such systems we need to choose whether the vacuum outside the system has the same or opposite Chern number as the one-dimensional system, i.e., whether $\lambda\lambda_0 = 1$ or -1, as discussed in Sec. II. This determines whether the wire hosts edge states. For the realization described above, one may toggle between the two cases by flipping the direction of the magnetic impurities defining the channel. The qualitative behavior of the system turns out to be the same irrespective of whether the wire hosts edge states.

We begin with typical results, illustrated in Figs. 3(a)–3(d) for a 50-Å-wide system, choosing Hamiltonian parameters and Fermi energies such that the subbands are reasonably well separated in energy and that a small number of transverse subbands are occupied in the ground state. Figures 3(a) and 3(b) illustrate results for boundary conditions in which there are no edge states ($\lambda\lambda_0 = 1$.) One observes several gapless plasmons, which at long wavelengths disperse linearly with momentum, as expected for this model. The gapless modes illustrated all lie above the energies of the particle-hole

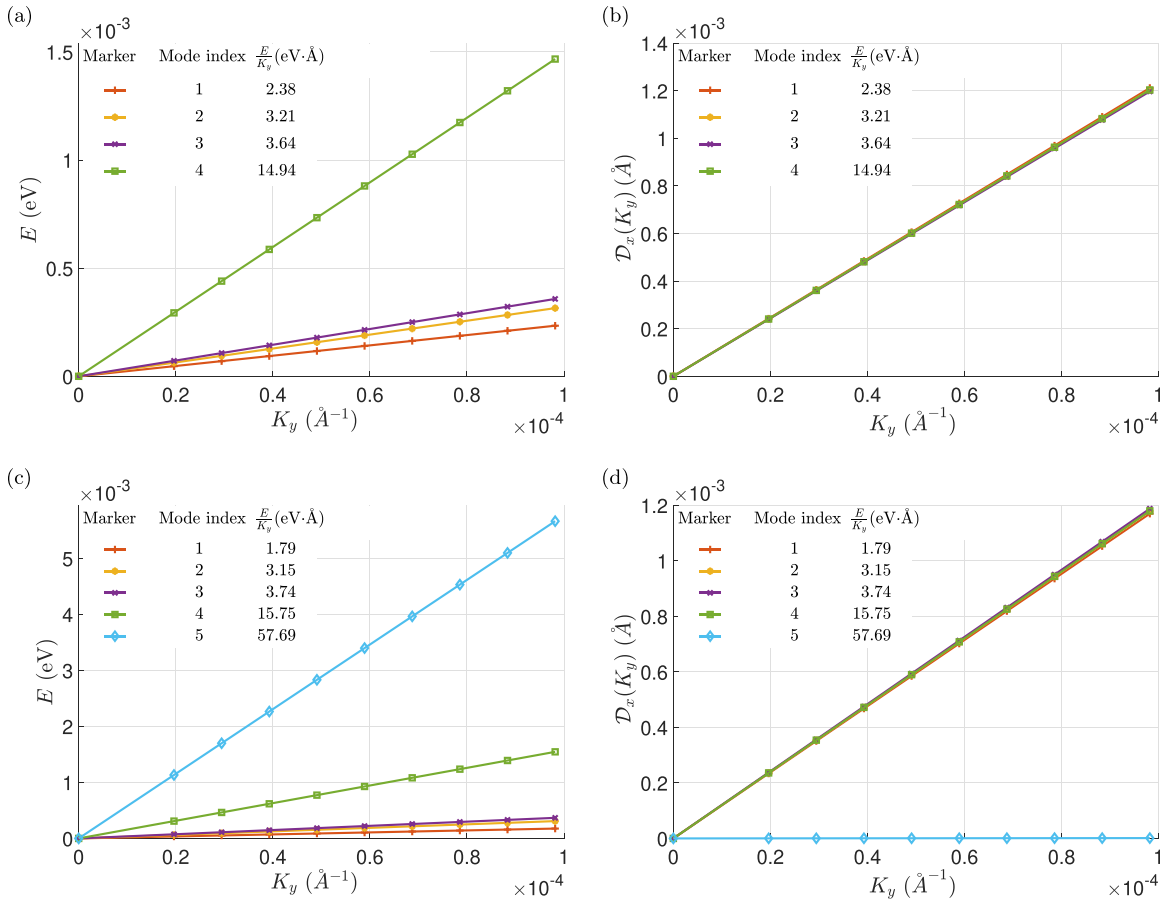

FIG. 4. Intraband plasmon energy and transverse dipole moments for K valley excitations. Parameters are given by $L = 86$Å, $\Delta = 1.6$ eV, $v_F\hbar = 3.94$ eVÅ, Fermi energy $\varepsilon_F = 1.007$ eV. (a) Intraband plasmon energies when four subbands are occupied. (b) Transverse dipole moments corresponding to (a). (c) Intraband plasmon energies when five modes are occupied (including edge states). (d) Transverse dipole moments corresponding to (c).

continuum. In general, the number of gapless modes is equal to the number of occupied subbands; we demonstrate this explicitly for the case of two occupied subbands in Appendix B. Importantly, all the plasmon modes exhibit nonvanishing transverse dipole moments, with magnitudes proportional to the plasmon momentum. As we discuss below, while this behavior is consistent with the (two-dimensional) quantum geometric properties of the system hosting the wire, it can be present in the wire geometry even when absent in the corresponding two-dimensional system.

An interesting possibility for these systems is that they may host edge states. These appear in our system when $\lambda\lambda_0 = -1$. As explained above, because of their physical location, one might expect them to have notable consequences for the transverse dipole moments of the nanoribbons. In fact, we find that for these kinds of generic parameters, the qualitative results are largely unaffected by the presence of edge states. This is illustrated in Figs. 3(c) and 3(d). We see the results are qualitatively rather similar to those of Figs. 3(a) and 3(b).

Surprising behavior of the transverse dipole moment emerges for systems with relatively large gaps. Figure 4(a) illustrates such a case, in which the Hamiltonian parameters have been chosen to model a single valley of WSe_2 [42] and $\lambda\lambda_0 = 1$ (no edge states on the wire). Figure 4(b) illustrates the transverse dipole moment of these plasmon modes. Remarkably, one finds essentially the same value for all the modes. This can be understood by close examination of the expression for the plasmon dipole for small-momentum K_y, which we show in Appendix C to have the form

$$\mathcal{D}_x(K_y) = \sum_\tau \frac{\tau K_y(Lm + \lambda_0\tau)}{2\varepsilon_F^3} \sum_n \sum_{k_y,s} \frac{|a_{n,n,\tau,s}(k_y; K_y)|^2}{L + \frac{\lambda_0\tau m}{m^2 + k_x(n)^2}} + \mathcal{O}(K_y^2), \tag{28}$$

where $k_x(n)$ is the quantized transverse momentum of the nth subband. Note that in this expression, in the present case where we consider a single valley (indexed by τ), one may set $\lambda\lambda_0 = \tau\lambda_0$. In situations where the gap parameter m is large, the last term in the denominator becomes negligible, so that the remaining sum $\sum_n \sum_{k_y,\tau,s} |a_{n,n,\tau,s}(k_y; K_y)|^2$ is determined *only* by the normalization of the plasmon wave function, and the resulting dipole moment becomes independent of the specific plasmon mode.

Figures 4(c) and 4(d) illustrate the corresponding results for the same parameters but with $\lambda\lambda_0 = -1$. In this case the systems host edge states in addition to the confined single-particle states, so that there are five occupied subbands. Here all but one of the plasmon modes host the same nonvanishing dipole moment, while the remaining mode does not. The result

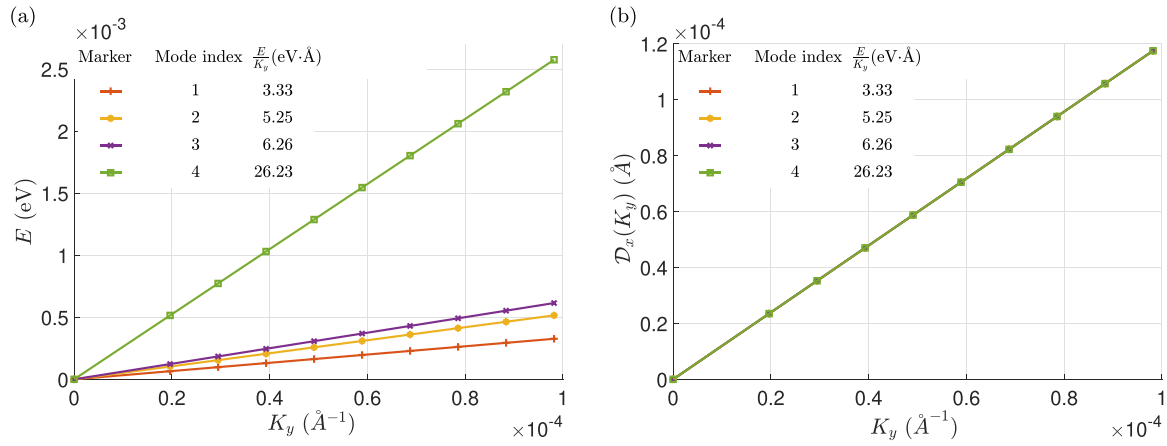

FIG. 5. Intraband plasmon energies and transverse dipole moments for K valley excitations in a situation where four subbands are occupied for a gapless chiral fermion. Parameters are $L = 50$Å, $\Delta = 0$ eV, $v_F\hbar = 3.94$ eVÅ, Fermi energy $\varepsilon_F = 1.007$ eV. (a) Plasmon energies. (b) Corresponding transverse dipole moments.

again can be understood from Eq. (28). In this case one finds that the mode with vanishing dipole moment has nearly all its weight in the edge state, for which $k_x(n) \approx im$, so that the denominator becomes divergent. More physically, because of the relatively large gap, the penetration length of the edge state into the bulk becomes independent of k_y, as does the single-particle transverse wave function. In this case the plasmon cannot sustain a transverse dipole moment. It is interesting to note that the difference in behaviors apparent in Figs. 4(b) and 4(d) in principle offers a way to distinguish when the one-dimensional channel is in a topological setting from a situation in which it is not: with the application of a transverse electric field coupling to the dipole moment, the energies and corresponding velocities of all the plasmon modes would shift in the nontopological case, whereas in the topological case one of these modes will be insensitive to the electric field.

B. Relationship to two-dimensional QGD

While the presence of an intrinsic dipole moment associated with plasmons in these one-dimensional systems is consistent with the presence of a QGD $\boldsymbol{\mathcal{D}}$ in their two-dimensional realizations [40], it is not necessary for $\boldsymbol{\mathcal{D}} \neq 0$ for these one-dimensional plasmons to carry a transverse dipole moment. Figures 5(a) and 5(b) illustrate this for the situation in which the gap parameter m vanishes, so that $\boldsymbol{\mathcal{D}} = 0$ for plasmons in this system in two dimensions [40]. Clearly one finds a nonvanishing transverse dipole for such plasmons, and indeed the results are qualitatively similar to those found for $\lambda\lambda_0 = 1$. Note that one does not expect the one-dimensional system to host edge states when $\Delta = 2m = 0$.

While for these relatively narrow systems we see little difference in the behavior of one-dimensional plasmons between systems in which $\boldsymbol{\mathcal{D}} \neq 0$ and $\boldsymbol{\mathcal{D}} = 0$, the distinction becomes relevant as the conducting channel gets wider. We illustrate this by computing the plasmon transverse dipole moment both for a chiral fermion system with vanishing gap ($m = 0$), for which $\boldsymbol{\mathcal{D}}$ vanishes [40], and for a gapped chiral fermion, for which it does not, and examine the plasmon behavior as the width L increases while the Fermi energy ε_F is held fixed. Figure 6(a) illustrates the behavior of the velocity of the fastest plasmon for a system with $m = 0$, and the associated dipole moment can be seen to vanish as L becomes large [Fig. 6(b)]. Figures 6(c) and 6(d) illustrate the corresponding quantities for a system with $m \neq 0$, for which the transverse dipole moment matches onto the (two-dimensional) quantum geometric dipole magnitude $|\boldsymbol{\mathcal{D}}|$. The robustness of the plasmon dipole moment with increasing L is thus a signature of its quantum geometric nature.

C. Multiple valleys: Vanishing dipole for time-reversal symmetric systems

While the systems discussed above involve relatively simple Hamiltonians, their physical realizations require time-reversal symmetry breaking, for example, via ferromagnetic insulating films which would need to be patterned onto the surface of a topological insulator. A much simpler system to realize would be a nanoribbon of transition-metal dichalcogenide (TMD) material, which in most cases preserves time-reversal symmetry. Such systems typically have two valleys, which are time-reversal partners of one another. With time-reversal symmetry intact, one does not expect plasmon modes to carry an intrinsic dipole moment. Figures 7(a) and 7(b) illustrate such a situation.

Nonvanishing dipole moments in such systems can be induced by breaking the symmetry between valleys. In TMD materials, spin-orbit coupling leads to a splitting between spin-up and spin-down states in opposite directions for the two valleys [42], so that a magnetic field imbalances the populations of the valleys through the Zeeman coupling. For magnetic fields that are not too large, such that the magnetic length $\ell = \sqrt{\hbar c/eB}$, with B the magnetic field, larger than the ribbon width, the orbital motion of the electrons will largely be unaffected by the field. To a good approximation one then only needs to include the spin dependence of the Fermi surfaces to account for the field.

Figures 7(c) and 7(d) illustrate such a situation in a ribbon of width $L = 50$ Å, for system parameters modeled after the hole bands of WSe_2, with a magnetic field $B = 10$ T, for which $\ell \approx 81$ Å. While the bands for each valley have the

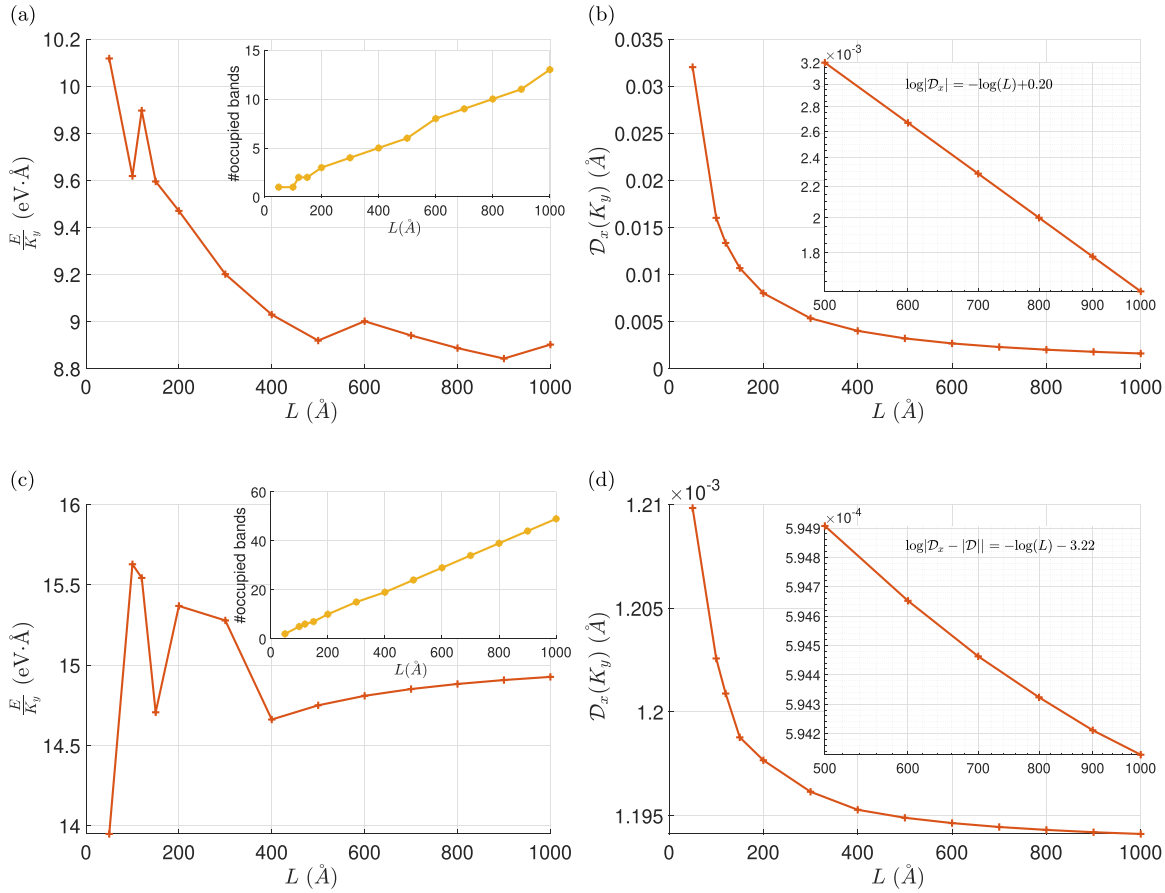

FIG. 6. Single-valley intraband plasmon velocity $\frac{E}{K_y}$ and transverse dipole moment evaluated at fixed plasmon momentum $K_y = 9.8 \times 10^{-5}$ Å^{-1}. Results are shown for the highest energy intraband plasmon. (a) Plasmon velocity for fixed Fermi energy 0.252 eV with zero gap. Horizontal axis shows the width of the wire. The energy gap is set to zero, so that a two-dimensional quantum geometric dipole $\boldsymbol{\mathcal{D}}$ vanishes. The cusps in the curve correspond to level anticrossings. (b) Transverse plasmon dipole moments corresponding to (a). Inset is a log-log plot of the same results. This quantity extrapolates to zero in this case. (c) Plasmon velocity for fixed Fermi energy 1.007 eV. Horizontal axis shows the width of the wire. The energy gap is that of the WSe_2, i.e., $\Delta = 2m = 1.60$ eV. The cusps in the curve correspond to level anticrossings. (d) Transverse plasmon dipole moments corresponding to (c). Inset is a log-log plot of the same results. The $L \to \infty$ value of the dipole moment $|\boldsymbol{\mathcal{D}}| \approx 6.00 \times 10^{-4}$ for these system parameters. The limiting value is the same as the two-dimensional QGD.

same dispersion, the Zeeman coupling leads to a difference of ∼8 meV in the extrema of the K and K' bands, yielding different carrier populations in each of them. While this leads to little change in the plasmon dispersions [compare Figs. 7(a) and 7(c)], the plasmons now carry dipole moments with small magnitudes [Fig. 7(d)]. Interestingly, these dipole moments can have either sign. At the more extreme end, this effect can used to completely depopulate one of the valleys of carriers. This situation is illustrated in Figs. 8(a) and 8(b). Interestingly, this yields a plasmon dipole moment that is relatively large.

V. SUMMARY AND DISCUSSION

In some two-dimensional conducting systems, plasmon excitations come with an intrinsic dipole moment that is quantum geometric in nature [40]. In this work we have explored conditions under which this kind of dipole moment might be found for quasi-one-dimensional geometries of the corresponding systems, using an RPA approach. Our studies focused on chiral fermions, as might be found on the surface of a topological insulator, or in two-dimensional van der Waals materials such as graphene or TMDs, and we adopted a simplified model with infinite mass boundary conditions at the system edges. We found that the presence of a transverse dipole moment is more ubiquitous in the wire geometry than in the two-dimensional system: the opening of a gap in the spectrum due to transverse confinement is sufficient to stabilize it, even when the corresponding gapless spectrum has no such dipole moment in two dimensions. The connection with the quantum geometric dipole is made by considering the wide wire limit, for which the plasmons retain dipole moments when the corresponding two-dimensional system has a nonvanishing quantum geometric dipole.

These plasmons differ from the corresponding modes of more conventional semiconducting quantum wires (e.g., GaAs): the topological character of the chiral fermions allow the possibility that they support edge states, which we find are present for sufficiently wide wires. Their presence increases the number of gapless plasmon modes supported by

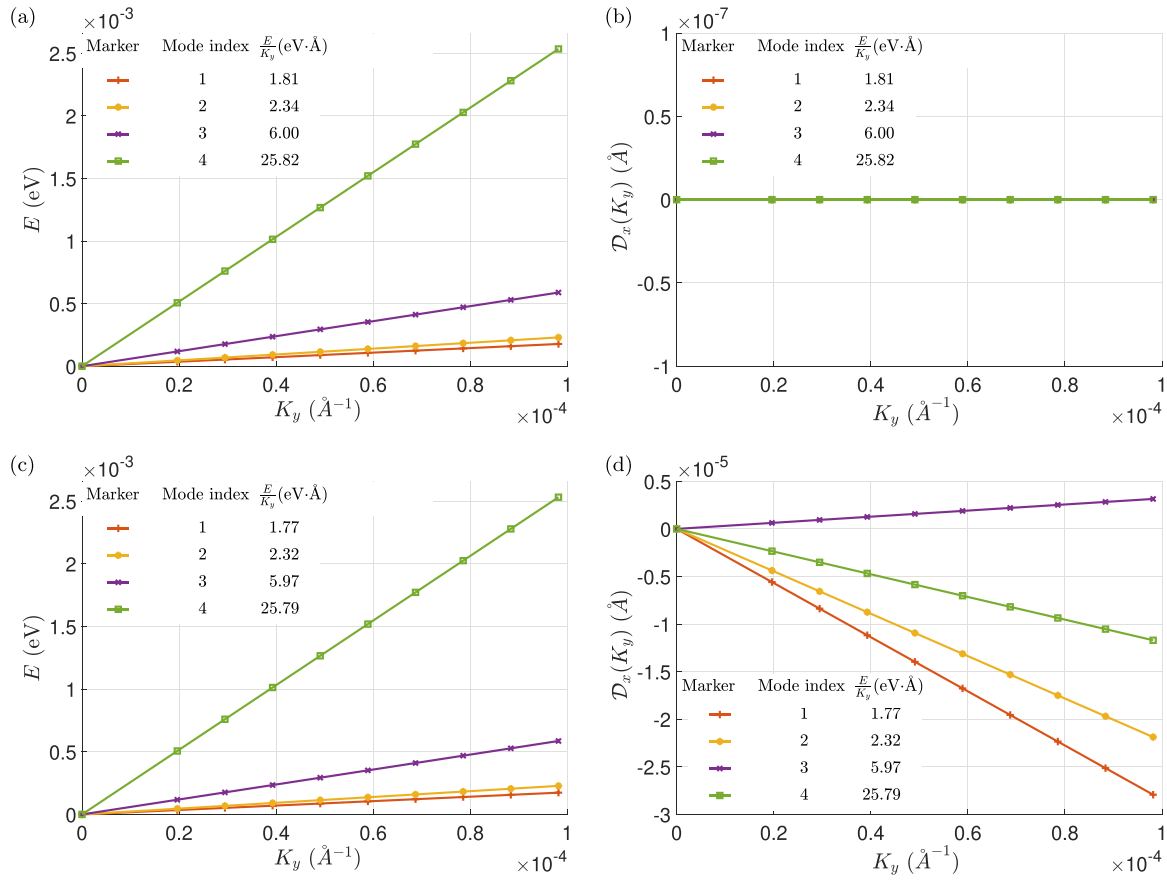

FIG. 7. Intraband plasmon energies and associated transverse dipole moments when two valleys that are time-reversal partners are retained. $L = 50$Å, $\Delta = 1.6$ eV, $v_F\hbar = 3.94$ eVÅ. (a) Plasmon energies when two subbands are occupied in each valley. The Fermi energy $\varepsilon_F = 1.008$ eV. (b) Transverse dipole moment corresponding to (a). Due to the symmetry, all the plasmon modes have vanishing dipole. (c) Plasmon energies for imbalanced valleys where two subbands are occupied in each valley. Fermi energy in the K valley is $\varepsilon_F(\tau = 1) = 1.008$ eV, while in the K' valley $\varepsilon_F(\tau = -1) = 1.000$ eV. The different effective Fermi energies can be induced by a magnetic field coupling to electron spins. (d) Transverse dipole moments corresponding to (c). Due to broken valley symmetry, all the plasmon modes yield a nonvanishing dipole.

the systems, but they only differ in their qualitative behavior for systems with relatively large gaps. In this limit we found that the dipole moments of the plasmon modes supported by the transverse confined states became degenerate across the modes, whereas a single plasmon associated with the edge states has vanishing dipole moment.

Single chiral fermion flavors can only be found in systems with broken time-reversal symmetry. In principle, a

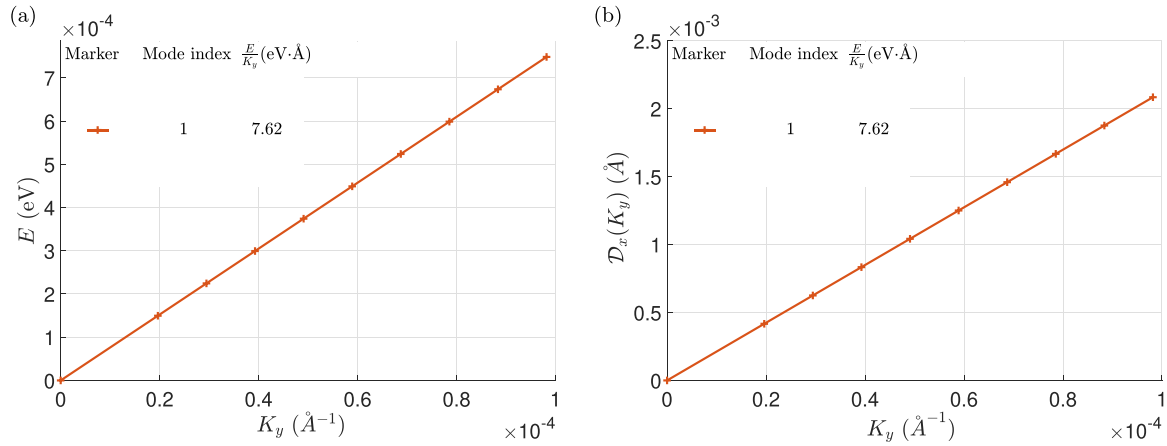

FIG. 8. Plasmon energies and transverse dipole moments in a 50-Å wire with Fermi energy $\varepsilon_F = -0.838$ eV for a typical TMD (WSe_2) half gap of 0.8 eV and Zeeman splitting of 8 meV. The boundary condition is chosen so that there are no edge modes. Only one subband of one valley is occupied in this situation. (a) Plasmon energies. (b) Transverse dipole moments.

conducting channel of these could be fabricated on the surface of topological insulator with ferromagnetically ordered magnetic ions on its surface, with a one-dimensional channel cut through. Systems with both chiral fermions and time-reversal symmetry support multiple flavors of chiral fermions (valleys), which are time-reversal partners of one another. Plasmons in these systems do not carry dipole moments. However, in TMDs they can be induced by the introduction of a magnetic field, which due to spin-orbit coupling imbalances the carrier populations in different valleys. For low carrier densities one may find complete depletion of some valleys, leading to relatively large transverse dipole moments in the plasmons.

A transverse dipole moment associated with a plasmon in a nanowire will in principle be signaled by a sensitivity of its frequency and speed to the application of a transverse electric field [54]: these will both vary linearly with electric field. For example, for the system parameters considered in Figs. 8(a) and 8(b), an external electric field of 0.01 V Å^{-1} will modify the speed of the plasmon by approximately 3.2×10^6 m/s and its energy by approximately 3%. Control of plasmon energies in such a continuous way in a single system could in principle bring new capabilities to plasmonic systems incorporating such nanowires.

Our studies suggest further directions for exploration. Beyond the gapless plasmons we have focused on in this work, nanowires support gapped, intersubband plasmons at higher frequencies [52]. Preliminary work [62] indicates that these also obtain nonvanishing dipole moments in chiral fermion settings, and they offer a way to detect this physics at higher frequencies. One may also consider the presence and role of transverse dipole moments in more complicated settings than considered in this work. For example, understanding the behavior of nanowire plasmons for other classes of boundary conditions, in particular those for which valley mixing is induced at the single-particle level [46,48], would likely be important for many types of nanowires. While we expect more realistic boundary conditions to modify details of the transverse dipole moment when the two valleys are coupled, a nonvanishing value should still be expected when time-reversal symmetry is broken. In particular, for systems where the chiral fermions have a nonvanishing mass in their Hamiltonians, we expect a transverse dipole moment to be particularly stable with respect to boundary conditions at the edge. The robustness of the effect in this case is emphasized by the results illustrated in Fig. 6, where we see the transverse dipole moment limits to the two-dimensional value for wide ribbons. This suggests that bulk behavior plays an important role in this physics.

Finally, one may also consider the effects of transverse dipole moments on plasmon nanochannel networks, which arise naturally in moiré superlattices, and which have been shown to support their own unique dynamics [25,29,30]. Such systems under some circumstances may become spontaneously valley-polarized, opening another avenue for the broken time-reversal symmetry needed for transverse dipole moments.

Plasmon modes can be generally understood as collective oscillations of the electric dipole moments of conducting systems. That such oscillations can occur with a static component which depends on the plasmon momentum is a relatively new insight, allowing the possibility of new physical phenomena. Nanowires offer a setting in which the direction of these dipole moments are fixed so that they can be interrogated with electric fields. For systems that support them, we expect they will admit new plasmonic phenomena of fundamental interest.

ACKNOWLEDGMENTS

L.B. acknowledges funding from PGC2018-097018-B-I00 (MICIN/AEI/FEDER, EU). H.A.F. and J.C. acknowledge the support of the NSF through Grants No. DMR-1914451 and No. ECCS-1936406. H.A.F. acknowledges support from the US-Israel Binational Science Foundation (Grants No. 2016130 and No. 2018726) of the Research Corporation for Science Advancement through a Cottrell SEED Award.

APPENDIX A: NANOWIRE WITH INFINITE MASS BOUNDARY CONDITION

In order to model chiral Dirac fermions confined to a quasi-one-dimensional channel, we consider a two-dimensional system with a position-dependent mass term:

$$\tilde{m}(x) = \begin{cases} m, & 0 < x < L, \\ V_0, & x < 0 \text{ or } x > L. \end{cases}$$

The Hamiltonian of the system is, in general,

$$H = \begin{pmatrix} \tilde{m} & i\tau k_x - ik_y \\ i\tau k_x + ik_y & -\tilde{m} \end{pmatrix},$$

where τ is the valley index. We find stationary states by matching eigenstates of H in the regions $-\infty < x < 0$ (region I), $0 \leqslant x \leqslant L$ (region II), and $x > L$ (region III) at the locations $x = 0$ and $x = L$. We ultimately take the limit $V_0 \to \pm\infty$ (infinite mass boundary conditions [50]), but some care must be taken with regard to whether the Chern numbers in the central and outer regions are the same or different. These Chern numbers are given by $C = \tau\,\mathrm{sgn}(m)/2$, so that the two cases are distinguished by the sign of mV_0. For the regions outside the nanowire, we denote the sign of the Chern numbers by $\lambda_0 \equiv \mathrm{sgn}(\tau V_0)$. Outside the wire one has for region I

$$\psi^I(\vec{r}) = C_1 \begin{pmatrix} V_0 + E \\ i(-\tau_0 k_1 + k_y) \end{pmatrix} e^{k_1 x + i k_y y},$$

with $k_1^2 = V_0^2 - E^2 + k_y^2$, where E is the energy of the state, while in region III,

$$\psi^{III}(\vec{r}) = C_3 \begin{pmatrix} V_0 + E \\ i(\tau_0 k_3 + k_y) \end{pmatrix} e^{-k_3 x + i k_y y},$$

with $k_3^2 = V_0^2 - E^2 + k_y^2$. Writing the upper and lower components of the spinors as ψ_1 and ψ_2, respectively, with the limit $|V_0| \to \infty$ we obtain [50]

$$\left.\frac{\psi_1}{\psi_2}\right|_{x=0} = i\lambda_0, \qquad \left.\frac{\psi_1}{\psi_2}\right|_{x=L} = -i\lambda_0. \tag{A1}$$

In the interior of the wire (region II), the general form of the wave function is

$$\psi_{\vec{k}}(\vec{r}) = \frac{e^{ik_y y}}{\sqrt{2E(E+m)}} \times \left[A \begin{pmatrix} E+m \\ \tau k_x + i k_y \end{pmatrix} e^{ik_x x} + B \begin{pmatrix} E+m \\ -\tau k_x + i k_y \end{pmatrix} e^{-ik_x x} \right], \tag{A2}$$

with A and B constants to be determined. Using Eqs. (A1) one finds

$$\frac{A}{B} = -\frac{E+m-i\lambda_0(-\tau k_x + i k_y)}{E+m-i\lambda_0(\tau k_x + i k_y)} \tag{A3}$$

and

$$\frac{A}{B} = -e^{-2ik_x L}\frac{E+m+i\lambda_0(-\tau k_x + i k_y)}{E+m+i\lambda_0(\tau k_x + i k_y)}. \tag{A4}$$

These two equations are consistent provided

$$e^{2ik_x L} = \frac{m - i\lambda_0 \tau k_x}{m + i\lambda_0 \tau k_x} = e^{-2i\lambda_0 \tau \arctan(\frac{k_x}{m})},$$

or equivalently,

$$k_x L = -\lambda_0 \tau \arctan\left(\frac{k_x}{m}\right) + n\pi.$$

Using Eqs. (A3) and (A4), one obtains the expressions

$$A \equiv A(\tau;\vec{k}) = \tau N \sqrt{(E+m)^2 + (\tau k_x - i k_y)^2}\sqrt{m + i\lambda_0 \tau k_x},$$

and

$$B \equiv B(\tau;\vec{k}) = -\tau N \sqrt{(E+m)^2 + (\tau k_x + i k_y)^2}\sqrt{m - i\lambda_0 \tau k_x},$$

where N is a normalization constant,

$$N = \left\{ 8L_y E(E+m)^2 \left[L\left(m^2 + k_x^2\right) + \lambda_0 \tau m \right] \right\}^{-1/2},$$

with L_y the length of the one-dimensional region.

In addition to these confined states, the wire edges may support edge states. This can occur only if the Chern numbers of the interior and exterior regions have different Chern numbers, which occurs when

$$\lambda\lambda_0 = -1,$$

with $\lambda = \tau\,\mathrm{sgn}(m)$. One finds these states by considering states that are evanescent not just in regions I and III but also in region II. These have the form

$$\psi^{II}(\vec{r}) = A \begin{pmatrix} m+E \\ i(\tau k_x + k_y) \end{pmatrix} e^{-k_x x + i k_y y} + B \begin{pmatrix} m+E \\ i(-\tau k_x + k_y) \end{pmatrix} e^{k_x x + i k_y y},$$

where $k_x^2 = m^2 - E^2 + k_y^2$. Applying Eqs. (A1) gives

$$\frac{A(m+E) + B(m+E)}{A(\tau k_x + k_y) - B(\tau k_x - k_y)} = -\lambda_0, \tag{A5}$$

$$\frac{A(m+E)e^{-k_x L} + B(m+E)e^{k_x L}}{A(\tau k_x + k_y)e^{-k_x L} - B(\tau k_x - k_y)e^{k_x L}} = \lambda_0. \tag{A6}$$

By eliminating A and B in Eqs. (A5) and (A6), we arrive at a transcendental equation for k_x:

$$e^{-2k_x L} = \frac{|m| + \lambda_0 \lambda k_x}{|m| - \lambda_0 \lambda k_x}. \tag{A7}$$

Equation (A7) may be solved if and only if $\lambda_0\lambda = -1$ and $mL > 1$. These are the conditions under which the quasi-one-dimensional system hosts edge states. Using Eqs. (A5) and (A6), the explicit forms for the coefficients turn out to be

$$A \equiv A_0(\tau) = \tau \sqrt{\frac{[(m+E)^2 - (\tau k_x - k_y)^2](m + k_x)}{8E(E+m)^2 L_y \left[m - L\left(m^2 - k_x^2\right)\right]}}$$

and

$$B \equiv B_0(\tau) = -\tau \sqrt{\frac{[(m+E)^2 - (\tau k_x + k_y)^2](m - k_x)}{8E(E+m)^2 L_y \left[m - L\left(m^2 - k_x^2\right)\right]}}.$$

APPENDIX B: ANALYTICAL SOLUTION FOR INTRABAND PLASMONS AT SMALL MOMENTUM

The appearance of multiple plasmon modes may appear surprising. In this section we show that this is to be expected, given the structure of the transverse wave functions for the systems we consider. To do this we first develop an alternative, equivalent formalism by which one may find the plasmon excitations and then apply it to the simple situation of two occupied subbands to show that there is more than a single gapless plasmon mode.

1. Equivalent dielectric formalism

For simplicity, we consider a massless chiral fermion system ($m = 0$), which is equivalent to a single valley of graphene, for which we set $\tau = 1$. First, we start from Eq. (24) and obtain the equivalent dielectric formalism for calculating the plasmon frequency. The contact interaction matrix element may be written in the form

$$V_{n_1,n_2,n_3,n_4}(k_{y1}, k_{y2}, k_{y3}, k_{y4}) = \frac{u_0}{2} L_y \int_0^L dx \left[\left(\vec{A}^{\dagger}_{n_1,k_{y1}} e^{-ik_x(n_1)x} + \vec{B}^{\dagger}_{n_1,k_{y1}} e^{ik_x(n_1)x} \right) \cdot \left(\vec{A}_{n_4,k_{y4}} e^{ik_x(n_4)x} + \vec{B}_{n_4,k_{y4}} e^{-ik_x(n_4)x} \right) \right], \times \left[\left(\vec{A}^{\dagger}_{n_2,k_{y2}} e^{-ik_x(n_2)x} + \vec{B}^{\dagger}_{n_2,k_{y2}} e^{ik_x(n_2)x} \right) \cdot \left(\vec{A}_{n_3,k_{y3}} e^{ik_x(n_3)x} + \vec{B}_{n_3,k_{y3}} e^{-ik_x(n_3)x} \right) \right],$$

where the spinor coefficients $\vec{A}_{n,k_y}$ and $\vec{B}_{n,k_y}$ may be read off from Eq. (A2), and $k_x(n)$ are the quantized wave vectors defined in Appendix A. By defining

$$f^{\sigma_1,\sigma_2,\sigma_3,\sigma_4}_{n_1,n_2,n_3,n_4} \equiv \int_0^L dx e^{-i\sigma_1 k_x(n_1)x - i\sigma_2 k_x(n_2)x + i\sigma_3 k_x(n_3)x + i\sigma_4 k_x(n_4)x}$$

and

$$\vec{D}_{n,k_y,\sigma} \equiv \begin{cases} \vec{A}_{n,k_y}, & \sigma = 1, \\ \vec{B}_{n,k_y}, & \sigma = -1, \end{cases}$$

the interaction matrix elements can be written in the compact form

$$\begin{aligned} &V_{n_1,n_2,n_3,n_4}(k_{y1}, k_{y2}, k_{y3}, k_{y4}) \\ &= \frac{u_0}{2} L_y \sum_{\sigma_1,\sigma_2,\sigma_3,\sigma_4} \left[\vec{D}^\dagger_{n_1,k_{y1},\sigma_1} \cdot \vec{D}_{n_4,k_{y4},\sigma_4}\right] \\ &\quad \times \left[\vec{D}^\dagger_{n_2,k_{y2},\sigma_2} \cdot \vec{D}_{n_3,k_{y3},\sigma_3}\right] f^{\sigma_1,\sigma_2,\sigma_3,\sigma_4}_{n_1,n_2,n_3,n_4}. \end{aligned}$$

In the single-valley case, the self-consistent equation for the plasmon wave function [Eq. (24)] can now be written as

$$\begin{aligned} a_{m_1,m_2,}(k'_y; K_y) = &\frac{u_0 L_y}{\omega_{k_y} - \varepsilon_{m_1}(k'_y + K_y) + \varepsilon_{m_2}(k'_y)} \sum_{n_2,n_3,k_{y1}} \sum_{\sigma_1,\sigma_2,\sigma_3,\sigma_4} \\ &\times \left[\vec{D}^\dagger_{m_1,k'_y+K_y,\sigma_1} \cdot \vec{D}_{m_2,k'_y,\sigma_4}\right] \left[\vec{D}^\dagger_{n_2,k_{y1},\sigma_2} \cdot \vec{D}_{n_3,k_{y1}+K_y,\sigma_3}\right] \\ &\times f^{\sigma_1,\sigma_2,\sigma_3,\sigma_4}_{m_1,n_2,n_3,m_2} [n_F(n_2, k_{y1}) - n_F(n_3, k_{y1} + K_y)] \\ &\times a_{n_3,n_2}(k_{y1}; K_y). \end{aligned}$$

Defining

$$\begin{aligned} \chi^{\sigma_1,\sigma_4}_{m_1,m_2}(K_y) \equiv &L_y \sum_{n_2,n_3,k_{y1}} \sum_{\sigma_2,\sigma_3} f^{\sigma_1,\sigma_2,\sigma_3,\sigma_4}_{m_1,n_2,n_3,m_2} \\ &\times \left[\vec{D}^\dagger_{n_2,k_{y1},\sigma_2} \cdot \vec{D}_{n_3,k_{y1}+K_y,\sigma_3}\right] [n_F(n_2, k_{y1}) \\ &- n_F(n_3, k_{y1} + K_y)] a_{n3,n_2}(k_{y1}; K_y) \end{aligned}$$

and

$$\xi_{m_1,m_2,k_y}(K_y) \equiv \sum_{\sigma_1,\sigma_2} \left[\vec{D}^\dagger_{m_1,k_y+K_y,\sigma_1} \cdot \vec{D}_{m_2,k_y,\sigma_2}\right] \chi^{\sigma_1,\sigma_2}_{m_1,m_2}(K_y),$$

one finds

$$\begin{aligned} &\xi_{m'_1,m'_2,k'_y}(K_y) \\ &= u_0 \sum_{m_1,m_2,k_y} \Bigg[L_y \sum_{\sigma'_1,\sigma'_2,\sigma_2,\sigma_1} f^{\sigma'_1,\sigma_2,\sigma_1,\sigma'_2}_{m'_1,m_2,m_1,m'_2} \\ &\quad \times \left[\vec{D}^\dagger_{m'_1,k'_y+K_y,\sigma'_1} \cdot \vec{D}_{m'_2,k'_y,\sigma'_2}\right] \left[\vec{D}^\dagger_{m_2,k_y,\sigma_2} \cdot \vec{D}_{m_1,k_y+K_y,\sigma_1}\right] \\ &\quad \times \frac{[n_F(m_2, k_y) - n_F(m_1, k_y + K_y)]}{\omega_{k_y} - \varepsilon_{m_1}(k_y + K_y) + \varepsilon_{m_2}(k_y)} \Bigg] \xi_{m_1,m_2,k_y}(K_y). \end{aligned} \tag{B1}$$

The quantity ξ may be understood as a dielectric function, with the expression inside the square brackets of Eq. (B1) representing a generalized polarization function $\Pi_{m_1,m_2,k_y;m'_1,m'_2,k'_y}(K_y, \omega)$. Nontrivial solutions to this equation must obey

$$\det[\mathbb{I} - u_0 \Pi(K_y, \omega)] = 0.$$

2. Intrasubband solutions for two subbands

We now show how this equation leads to multiple gapless plasmons. As a simplest concrete example we consider a massless chiral fermion system (e.g., single valley of graphene) with two subbands, both of which are occupied in the ground state, and include only intrasubband excitations in the analysis. In Eq. (B1) this entails retaining only pairs of indices satisfying $m_1 = m_2$ and $m'_1 = m'_2$. One then has

$$\begin{aligned} &\xi_{m'_1,m'_1,k'_y}(K_y) \\ &= u_0 L_y \sum_{m_1,k_y} \Bigg[\sum_{\sigma'_1,\sigma'_2,\sigma_2,\sigma_1} f^{\sigma'_1,\sigma_2,\sigma_1,\sigma'_2}_{m'_1,m_1,m_1,m'_1} \\ &\quad \times \left[\vec{D}^\dagger_{m'_1,k'_y+K_y,\sigma'_1} \cdot \vec{D}_{m'_1,k'_y,\sigma'_2}\right] \left[\vec{D}^\dagger_{m_1,k_y,\sigma_2} \cdot \vec{D}_{m_1,k_y+K_y,\sigma_1}\right] \\ &\quad \times \frac{[n_F(m_1, k_y) - n_F(m_1, k_y + K_y)]}{\omega_{k_y} - \varepsilon_{m_1}(k_y + K_y) + \varepsilon_{m_1}(k_y)} \Bigg] \xi_{m_1,m_1,k_y}(K_y). \end{aligned} \tag{B2}$$

The relevant spinors entering $\vec{D}$ can be evaluated as

$$\vec{A}_{n,k_y} = \frac{1}{\sqrt{8LL_y}} \frac{1}{\sqrt{k(k+k_y)}} \begin{pmatrix} k + k_y + ik_x \\ i(k + k_y - ik_x) \end{pmatrix}$$

and

$$\vec{B}_{n,k_y} = \frac{1}{\sqrt{8LL_y}} \frac{1}{\sqrt{k(k+k_y)}} \begin{pmatrix} -(k + k_y - ik_x) \\ -i(k + k_y + ik_x) \end{pmatrix},$$

where $k_x \equiv k_x(n)$ and $k = \sqrt{k_x^2 + k_y^2}$. We next note that for small K_y, the k_y momentum sums involve only very small intervals, so that one may set all the values of k_y in the various $\vec{D}_{m,k_y,\sigma}$ and $\vec{D}^\dagger_{m,k_y,\sigma}$ factors appearing in Eq. (B2) to their values where the subbands cross the Fermi energy, $k_y \to k_F(m)$, where $k_F(m) = \sqrt{\varepsilon_F^2 - [\hbar v_F k_x(m)]^2}/\hbar v_F$, with ε_F the Fermi energy and v_F the velocity of the chiral fermion. After some algebra, one finds

$$\sum_{\sigma'_1,\sigma'_2,\sigma_2,\sigma_1} f^{\sigma'_1,\sigma_2,\sigma_1,\sigma'_2}_{m'_1,m_1,m_1,m'_1} \left[\vec{D}^\dagger_{m'_1,k'_y+K_y,\sigma'_1} \cdot \vec{D}_{m'_1,k'_y,\sigma'_2}\right] \left[\vec{D}^\dagger_{m_1,k_y,\sigma_2} \cdot \vec{D}_{m_1,k_y+K_y,\sigma_1}\right] \approx \frac{1}{LL_y^2} \left[1 + \frac{1}{2} \frac{[\hbar v_F k_F(m_1)]^2}{\varepsilon_F^2} \delta_{m_1,m'_1}\right].$$

Specializing to the case of just two occupied subbands, using the notation $\xi_{m,m,k_F(m)} \to \xi_m$, one finds to linear order in K_y,

$$\begin{pmatrix}\xi_1(K_y)\\ \xi_2(K_y)\end{pmatrix} = v_0\begin{pmatrix}(1+\frac{k_F(1)^2}{2\varepsilon_F^2})I_1(K_y,\omega) & I_2(K_y,\omega)\\ I_1(K_y,\omega) & (1+\frac{k_F(2)^2}{2\varepsilon_F^2})I_2(K_y,\omega)\end{pmatrix}\begin{pmatrix}\xi_1(K_y)\\ \xi_2(K_y)\end{pmatrix},$$

where $v_0 = \frac{u_0\varepsilon_F}{K_y L}$, $v_F\hbar = 1$, and

$$I_m(K_y,\omega) = \frac{K_y}{\varepsilon_F}\int_{k_F(m)-K_y}^{k_F(m)} \frac{dk_y}{\omega_{k_y} - \varepsilon_m(k_y+K_y) + \varepsilon_m(k_y)}. \tag{B3}$$

Nontrivial solutions to Eq. (B3) exist when

$$\big[a_1 I_1(K_y,\omega) - v_0^{-1}\big]\big[a_2 I_2(K_y,\omega) - v_0^{-1}\big] - I_1(K_y,\omega)I_2(K_y,\omega) = 0, \tag{B4}$$

where $a_m = 1 + k_F(m)^2/2\varepsilon_F^2$.

For small K_y, Eq. (B3) can be evaluated directly. Writing the (noninteracting) speed of a particle along the wire in an occupied subband m at the Fermi energy as v_m, for small K_y one finds

$$I_m = \frac{K_y^2/\varepsilon_F}{\omega - v_m K_y}. \tag{B5}$$

Direct substitution of Eq. (B5) into Eq. (B4) generates a quadratic equation for ω in terms of K_y with solutions

$$\omega_\pm(K_y) = \tfrac{1}{2}\big\{v_1 + v_2 + (a_1+a_2)\tilde{u}_0 \pm \big[(v_2 + a_1\tilde{u}_0 - v_1 - a_2\tilde{u}_0)^2 + 4\tilde{u}_0^2\big]^{1/2}\big\}K_y,$$

where $\tilde{u}_0 \equiv u_0/L$. Thus we generate two nondegenerate collective modes with frequencies different from those of the noninteracting particle-hole excitations.

APPENDIX C: DEGENERACY OF TRANSVERSE DIPOLE MOMENTS

In Sec. IV A it was shown that under certain circumstances the transverse dipole moment $\mathcal{D}_x(K_y)$ can be the same for multiple plasmon modes at small K_y, even when the frequencies of these modes are quite different. This behavior is explained by Eq. (28), in which one may see that $\mathcal{D}_x(K_y)$ becomes independent of the details of plasmon wave function when $m \gg \hbar v_F k_x(n)$ for the subbands n involved in the plasmon wave function. [Note in Eq. (28), $\hbar$ and v_F have been set to 1.) In this Appendix we present some details of the derivation of Eq. (28).

Our starting point is Eq. (27), and we consider only intrasubband particle-hole excitations in constructing the low-energy plasmon wave functions. This means the quantities we need to focus on have the form

$$\vec{d}_m(k_y) = \int x\vec{\psi}^{\tau,*}_{m,k_y}(\vec{r})\cdot\vec{\psi}^{\tau}_{m,k_y}(\vec{r})d^2r.$$

Writing the plasmon wave functions, Eq. (4), in the form

$$\vec{\psi}^{\tau}_{\vec{k}}(\vec{r}) = \vec{A}_{m,k_y}e^{ik_x x + ik_y y} + \vec{B}_{m,k_y}e^{-ik_x x + ik_y y},$$

where $k_x \equiv k_x(m)$, one finds

$$\vec{d}_m(k_y) = \frac{L^2 L_y}{2}(|\vec{A}_{m,k_y}|^2 + |\vec{B}_{m,k_y}|^2) + 2L_y\mathrm{Re}(\vec{A}^\dagger_{m,k_y}\cdot\vec{B}_{m,k_y}) \times \int xe^{-2ik_x x}dx.$$

Reading off the forms of $\vec{A}_{m,k_y}$ and $\vec{B}_{m,k_y}$ from the wave functions in Sec. II, one finds

$$|\vec{A}_{m,k_y}|^2 = |\vec{B}_{m,k_y}|^2 = \frac{1}{2L_y}\frac{m^2+k_x^2}{L\big(m^2+k_x^2\big)+\lambda_0\tau m},$$

where we have set $\hbar = v_F = 1$. Remarkably, these combinations are independent of k_y; because $\vec{\mathcal{D}}(K_y)$ involves the difference of $\vec{d}_m(k_y)$ at two different k_y values, terms involving $|\vec{A}_{m,k_y}|^2$ and $|\vec{B}_{m,k_y}|^2$ do not contribute to the dipole moment of the plasmon. For small K_y, the transverse component of the dipole moment can now be written as $\mathcal{D}_x \equiv \sum_m \mathcal{D}_{x,m}$, where the sum is over occupied subbands, and

$$\mathcal{D}_{x,m}(K_y) = K_y\partial_{k_y}\left(2L_y\mathrm{Re}\left(\vec{A}^\dagger_{m,k_y}\cdot\vec{B}_{m,k_y}\int xe^{-2ik_x x}dx\right)\right)\Big|_{k_y=k_F} + \mathcal{O}(K_y)^2.$$

With some algebra one may show

$$\vec{A}^\dagger_{m,k_y}\cdot\vec{B}_{m,k_y} = -\frac{(mE + i\tau k_x k_y)(m - i\lambda_0\tau k_x)}{2L_y E\big[L\big(m^2+k_x^2\big)+\lambda_0\tau m\big]},$$

and using this relation, after performing the integration one finds

$$2L_y\mathrm{Re}\left(\vec{A}^\dagger_{m,k_y}\cdot\vec{B}_{m,k_y}\int xe^{-2ik_x x}dx\right) = \frac{m\lambda_0\tau}{2\big[L\big(m^2+k_x^2\big)+\lambda_0\tau m\big]} + \frac{\tau k_y(Lm+\lambda_0\tau)}{2E\big[L\big(m^2+k_x^2\big)+\lambda_0\tau m\big]}.$$

The first term is independent of k_y and therefore does not contribute. Using

$$\partial_{k_y}\left(\frac{k_y}{E}\right)\Big|_{k_y=k_F} = \frac{m^2+k_x^2}{\varepsilon_F^3},$$

we arrive at

$$\mathcal{D}_{x,m}(K_y) = \frac{K_y}{2\varepsilon_F^3}\frac{\tau(Lm+\lambda_0\tau)}{L+\frac{\lambda_0\tau m}{m^2+k_x^2}} + \mathcal{O}\big(K_y^2\big).$$

Thus, to linear order in K_y, the transverse plasmon dipole moment is

$$\mathcal{D}_x(K_y) = \sum_\tau \frac{\tau K_y(Lm+\lambda_0\tau)}{2\varepsilon_F^3}\sum_n\sum_{k_y,s}\frac{|a_{n,n,\tau,s}(k_y;K_y)|^2}{L+\frac{\lambda_0\tau m}{m^2+k_x(n)^2}},$$

which is Eq. (28).

[1] D. Pines and P. Noziéres, *The Theory of Quantum Liquids: Normal Fermi Liquids* (W.A. Benjamin, New York, 1966).

[2] D. Bohm and D. Pines, Phys. Rev. **92**, 609 (1953).

[3] G. Giuliani and G. Vignale, *Quantum Theory of the Electron Liquid* (Cambridge University Press, Cambridge, 2005).

[4] C. Kittel, *Introduction to Solid State Physics*, 8th ed. (Wiley, New York, 2004), http://www.amazon.com/Introduction-Solid-Physics-Charles-Kittel/dp/047141526X/ref=dp_ob_title_bk.

[5] M. Dressel and G. Grüner, *Electrodynamics of Solids: Optical Properties of Electrons in Matter* (Cambridge University Press, Cambridge, 2002), https://www.cambridge.org/core/books/electrodynamics-of-solids/DFDDF1640793690DAFD338BFDD1A18BF.

[6] R. H. Ritchie, Phys. Rev. **106**, 874 (1957).

[7] J. M. Pitarke, V. M. Silkin, E. V. Chulkov, and P. M. Echenique, Rep. Prog. Phys. **70**, 1 (2007).

[8] T. Ando, A. B. Fowler, and F. Stern, Rev. Mod. Phys. **54**, 437 (1982).

[9] F. Stern, Phys. Rev. Lett. **18**, 546 (1967).

[10] S. Das Sarma, Phys. Rev. B **29**, 2334 (1984).

[11] B. Wunsch, T. Stauber, F. Sols, and F. Guinea, New J. Phys. **8**, 318 (2006).

[12] E. H. Hwang and S. Das Sarma, Phys. Rev. B **75**, 205418 (2007).

[13] A. N. Grigorenko, M. Polini, and K. S. Novoselov, Nat. Photonics **6**, 749 (2012).

[14] X. Luo, T. Qiu, W. Lu, and Z. Ni, Mater. Sci. Eng. R **74**, 351 (2013).

[15] H. Yu, Y. Wang, Q. Tong, X. Xu, and W. Yao, Phys. Rev. Lett. **115**, 187002 (2015).

[16] P. A. Gonçalves and N. Peres, *An Introduction to Graphene Plasmonics* (World Scientific Publishing, Singapore, 2016).

[17] E. Hutter and J. Fendler, Adv. Mater. **16**, 1685 (2004).

[18] J. S. Sekhon and S. S. Verma, Curr. Sci. **101**, 484 (2011).

[19] A. Y. Nikitin, F. Guinea, F. J. Garcia-Vidal, and L. Martin-Moreno, Phys. Rev. B **84**, 195446 (2011).

[20] K. S. Thygesen, 2D Mater. **4**, 022004 (2017).

[21] A. Agarwal, M. S. Vitiello, L. Viti, A. Cupolillo, and A. Politano, Nanoscale **10**, 8938 (2018).

[22] S. Linic, P. Christopher, and D. B. Ingram, Nat. Mater. **10**, 911 (2011).

[23] L. Ju, B. Geng, J. Horng, C. Girit, M. Martin, Z. Hao, H. A. Bechtel, X. Liang, A. Zettl, Y. R. Shen *et al.*, Nat. Nanotechnol. **6**, 630 (2011).

[24] E. Suárez Morell, L. Chico, and L. Brey, 2D Mater., **4**, 035015 (2017).

[25] T. Stauber, T. Low, and G. Gómez-Santos, Nano Lett. **20**, 8711 (2020).

[26] A. Woessner, M. B. Lundeberg, Y. Gao, A. Principi, P. Alonso-González, M. Carrega, K. Watanabe, T. Taniguchi, G. Vignale, M. Polini *et al.*, Nat. Mater. **14**, 421 (2015).

[27] D. Alcaraz Iranzo, S. Nanot, E. J. C. Dias, I. Epstein, C. Peng, D. K. Efetov, M. B. Lundeberg, R. Parret, J. Osmond, J.-Y. Hong *et al.*, Science **360**, 291 (2018).

[28] D. Giri, D. K. Mukherjee, S. Verma, H. A. Fertig, and A. Kundu, arXiv:2011.06862.

[29] G. X. Ni, H. Wang, J. S. Wu, Z. Fei, M. D. Goldflam, F. Keilmann, B. Özyilmaz, A. H. Castro Neto, X. M. Xie, M. M. Fogler *et al.*, Nat. Mater. **14**, 1217 (2015).

[30] L. Brey, T. Stauber, T. Slipchenko, and L. Martín-Moreno, Phys. Rev. Lett. **125**, 256804 (2020).

[31] K. Sawada, K. A. Brueckner, N. Fukuda, and R. Brout, Phys. Rev. **108**, 507 (1957).

[32] M. Gell-Mann and K. A. Brueckner, Phys. Rev. **106**, 364 (1957).

[33] M. S. Tame, K. R. McEnery, Ş. K. Özdemir, J. Lee, S. A. Maier, and M. S. Kim, Nat. Phys. **9**, 329 (2013).

[34] J. M. Fitzgerald, P. Narang, R. V. Craster, S. A. Maier, and V. Giannini, Proc. IEEE **104**, 2307 (2016).

[35] S. I. Bozhevolnyi and J. B. Khurgin, Nat. Photonics **11**, 398 (2017).

[36] Z.-K. Zhou, J. Liu, Y. Bao, L. Wu, C. E. Png, X.-H. Wang, and C.-W. Qiu, Prog. Quantum Electron. **65**, 1 (2019).

[37] J. C. W. Song and M. S. Rudner, Proc. Natl. Acad. Sci. **113**, 4658 (2016).

[38] L.-k. Shi and J. C. W. Song, Phys. Rev. X **8**, 021020 (2018).

[39] M. Papaj and C. Lewandowski, Phys. Rev. Lett. **125**, 066801 (2020).

[40] J. Cao, H. A. Fertig, and L. Brey, Phys. Rev. Lett. **127**, 196403 (2021).

[41] J. Cao, H. A. Fertig, and L. Brey, Phys. Rev. B **103**, 115422 (2021).

[42] D. Xiao, G.-B. Liu, W. Feng, X. Xu, and W. Yao, Phys. Rev. Lett. **108**, 196802 (2012).

[43] M. S. Nevius, M. Conrad, F. Wang, A. Celis, M. N. Nair, A. Taleb-Ibrahimi, A. Tejeda, and E. H. Conrad, Phys. Rev. Lett. **115**, 136802 (2015).

[44] D. Jariwala, A. Srivastava, and P. M. Ajayan, J. Nanosci. Nanotechnol. **11**, 6621 (2011).

[45] M. V. Bollinger, J. V. Lauritsen, K. W. Jacobsen, J. K. Nørskov, S. Helveg, and F. Besenbacher, Phys. Rev. Lett. **87**, 196803 (2001).

[46] L. Brey and H. A. Fertig, Phys. Rev. B **73**, 235411 (2006).

[47] L. Brey and H. A. Fertig, Phys. Rev. B **73**, 195408 (2006).

[48] A. R. Akhmerov and C. W. J. Beenakker, Phys. Rev. B **77**, 085423 (2008).

[49] J. J. Palacios, J. Fernandez-Rossier, L. Brey, and H. A. Fertig, Semicond. Sci. Technol. **25**, 033003 (2010).

[50] M. V. Berry and R. Mondragon, Proc. R. Soc. London, Ser. A **412**, 53 (1987).

[51] L. Brey and H. A. Fertig, Phys. Rev. B **75**, 125434 (2007).

[52] Q. Li and S. D. Sarma, Phys. Rev. B **40**, 5860 (1989).

[53] G. Y. Hu and R. F. O'Connell, Phys. Rev. B **42**, 1290 (1990).

[54] M. Pizzochero, N. V. Tepliakov, A. A. Mostofi, and E. Kaxiras, Nano Lett. **21**, 9332 (2021).

[55] A. H. Castro Neto, F. Guinea, N. M. R. Peres, K. S. Novoselov, and A. K. Geim, Rev. Mod. Phys. **81**, 109 (2009).

[56] M. I. Katsnelson, *Graphene: Carbon in Two Dimensions* (Cambridge University Press, Cambridge, 2012), pp. i–v, https://www.cambridge.org/core/books/graphene/frontmatter/A99E4140C9F7D4E195FD6A2A470A0A36.

[57] S. M. Girvin and K. Yang, *Modern Condensed Matter Physics* (Cambridge University Press, Cambridge, England, 2019).

[58] S. Das Sarma and W.-y. Lai, Phys. Rev. B **32**, 1401 (1985).
[59] Q. P. Li and S. Das Sarma, Phys. Rev. B **43**, 11768 (1991).
[60] F. Karimi and I. Knezevic, Phys. Rev. B **96**, 125417 (2017).
[61] D. J. Thouless, *The Quantum Mechanics of Many-Body Systems*, 2nd Ed. (Academic Press, New York, 1972), Vol. 11, p. iii, https://www.sciencedirect.com/science/article/pii/B9781483230665500020.
[62] J. Cao, H. Fertig, and L. Brey (unpublished).